Jinghao Li, John F. Hunt*, Shaoqin Gong and Zhiyong Cai*

Fatigue behavior of wood-fiber-based tri-axial engineered sandwich composite panels (ESCP)

DOI 10.1515/hf-2015-0091
Received April 11, 2015; accepted October 20, 2015; previously published online xx

Abstract: The static and fatigue bending behavior of wood-fiber-based tri-axial engineered sandwich composite panels (ESCP) has been investigated by four-point bending tests. Fatigue panels and weakened panels (wESCP) with an initial interface defect were manufactured for the fatigue tests. Stress σ vs. number of cycles curves (S-N) were recorded under the different stress levels. The primary failure mode in the fatigue tests was observed in the shear zone (epoxy debonding), which was different from face failure in the pure bending zone for the static bending test. For residual bending (RB) test, epoxy debonding failure occurred between the pure bending zone and shear zone. Macro cracks along the core/face interface developed as the number of cycles increased during the fatigue life. The crack propagation or damage for the panels submitted to fatigue test can be described as a three-stage damage process of first non-linear portion, followed by linear damage accumulation, and lastly non-linear accelerated damage. Bending stiffness degradation at the higher load level had faster degradation during fatigue life. The dissipated energy of the panels was small due to the high stiffness of the materials.

Keywords: bending stiffness, fatigue behavior, residual properties, sandwich panel, S-N curve, static testing, wood-fiber-composite

***Corresponding authors: John F. Hunt, Zhiyong Cai,** USDA Forest Service, Forest Products Laboratory, Madison, WI 53726, USA, e-mail: jfhunt@fs.fed.us (J.F. Hunt), zcai@fs.fed.us (Z. Cai)
Jinghao Li: Department of Biomedical Engineering, Wisconsin Institutes for Discovery, and Department of Materials Science and Engineering, University of Wisconsin-Madison, Madison, WI 53715, USA; and USDA Forest Service, Forest Products Laboratory, Madison, WI 53726, USA
Shaoqin Gong: Department of Biomedical Engineering, Wisconsin Institutes for Discovery, and Department of Materials Science and Engineering, University of Wisconsin-Madison, Madison, WI 53715, USA

Introduction

Sandwich composite (SC) materials having a high strength to weight ratio are widely used for a variety of applications such as shipping, aerospace, building construction, and transportation (Davalos et al. 2001; Vasiliev et al. 2001; Sharaf and Fam 2011; Wei et al. 2013). They are fabricated based on a foam or honeycomb core between two stiff faces (Fan et al. 2007; Shalbafan et al. 2013; Smardzewski 2013). For some higher performance applications of SC panels (SCP), aluminum iso-grid cores have been used. Iso-grid structures were more efficient than either foam or honeycomb structures (Gibson and Ashby 1997). The ribs are aligned in different directions that better distribute the stress for multidirectional loadings. Bi-directional grids are the simplest structure in the iso-grid domain and provide the simplest manufacturing, whereas it offers little shear and twisting stiffness compared with a tri-grid or multi-grid core aligned structure. The tri-grid ribs have three different orientations to resist the shear stress (Han and Tsai 2003). Therefore, this type of structures with improved performance capabilities attracted a lot of interest (Huybrecht et al. 2002; Wodesenbet et al. 2003; Higgins et al. 2004; Zhang et al. 2005). Interlocked kagome grid SCPs were fabricated based on carbon fiber composites and their mechanical behavior was studied including out-of-panel, in-plane compression, and bending tests (Fan et al. 2007). The energy absorption characteristics of grid-stiffened fiberglass composites were also investigated under transverse loading. Gan et al. (2004) found that iso-grid structures have good damage tolerance where most of the energy absorption occurs beyond the initial failure. Cicala et al. (2012) investigated a truss-core structure made of hemp/epoxy biocomposite by tensile and flexural tests and found that this core exhibits better specific shear modulus and strength than a model made of polymeric core. Zuhri et al. (2014) focused on structural materials with either interlocked grid-core made of co-mingled flax-fiber reinforced polypropylene or polylactide polymers. The static compressive properties of these materials were modeled with finite elements (FE) to estimate the compressive response and energy-absorbing characteristics. However, the fatigue behavior of iso-grid structures is not well investigated.

Brought to you by | DigiTop - USDA's Digital Desktop Library
Authenticated
Download Date | 11/23/15 11:09 PM

The Forest Products Laboratory (FPL) develops bio-based engineered sandwich materials aiming at better a performance in various engineered applications including pallets or tactical shelters (Li et al. 2013, 2014, 2016a,b). There are many mid-level performance applications that require higher stiffness and some level of fire and water resistance. Therefore, phenolic laminated paper was selected as an initial wood-fiber-based composite material as part of tri-axial iso-grid sandwich panels. The search for some niche applications at reduced costs belongs also to the research goals. Compared to the other structural materials made of natural fiber (Zuhri et al. 2014), this tri-axial iso-grid structure with its large triangular cellular cores made from wood-fiber-based laminated paper has a significantly higher stiffness and may be advantageous in larger applications.

In sandwich type panels, face compression and core debonding are observed in case of both undamaged and initially weakened panels (wESCP) (Belingardi et al. 2007). The fatigue strength is dependent of the kind and amount of adhesive applied but the thickness of face sheet is not influential (Jen et al. 2009a,b). The failure mechanisms of composites have been investigated also by in-plane shear load-fatigue tests (Bianchi et al. 2012). The fatigue properties of engineered strand lumber and engineered strand panels have been studied and it was demonstrated that these materials could easily survive 10^6 load cycles if loaded to <40% ultimate strength levels (Eckelman and Winandy 1978). The fatigue behavior of oriented strand board (OSB) was tested by five-point load bending (Cai et al. 1996). Bao et al. (1996) compared the fatigue properties medium density fiberboard, particleboard, plywood, and oriented strand board. The non-linear behavior of fatigue and heating of wood was investigated by Nakano (1997).

However, no literature was found concerning the fatigue behavior of tri-axial engineered sandwich core panels (shortly: ESCP). This is the reason why in the present study, the fatigue behavior of ESCP (based on laminated paper) will be investigated by four-point bending fatigue. The focus will be the fatigue behavior of the panels, where the panels will be subjected to cyclic loading. The expectation is that the knowledge in terms of the mechanical characteristics of this type of sandwich panels will be better understood.

Materials and methods

Materials: Phenolic impregnated laminated paper (NP610) with the nominal thickness of 2.4 mm was obtained from Norplex-Micarta Inc. (Postville, IA, USA). In this context, the laminated paper's machine direction and cross-machine direction are designated as MD (x-axis) and CD (y-axis), respectively. Epoxy 635 resin is from US Composites (West Palm Beach, FL, USA), with a ratio of epoxy to hardener of 3:1.

Panel design: Tri-axial engineered sandwich core panels (ESCP) were prepared in the USDA, Forest Products Laboratory, WI, USA as illustrated in Figure 1a. The core nominal height with the linear ribs was 33.0 mm. The slots were cut slightly oversized to accommodate the 60° angular orientation between the ribs when assembled. The slot spacing was 117.3 mm, thus an equilateral triangle was created after assembling. Before applying epoxy resin as adhesive, all laminate paper face surfaces were first lightly sanded on the glue side, and then the resin was spread on the faces. A total of 18 panels were fabricated. The configuration includes three centrally located linear ribs (Figure 1a) with the spacing of 101.6 mm. Measures of the panel: span 914 mm, width 267 mm, and nominal thickness 38 mm (see Figure 1b). Three panels were tested by static bending. Twelve panels were tested by fatigue bending tests at four stress levels. Three panels were fabricated to simulate a "weakened" panel (wESCP) and to observe crack propagation without resin along a 100 mm portion of a

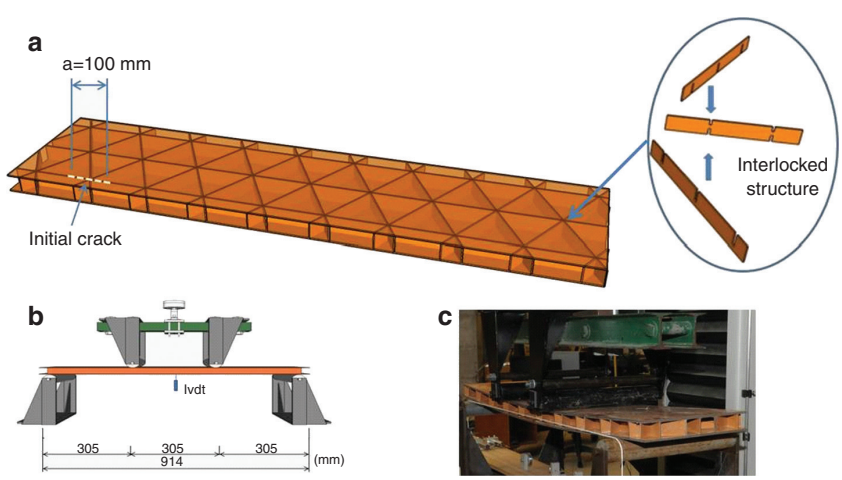

Figure 1: (a) The tri-axial sandwich configuration with an initial crack, (b) bending test dimensions, (c) panel under static load during a bending test.

Brought to you by | DigiTop - USDA's Digital Desktop Library
Authenticated
Download Date | 11/23/15 11:09 PM

rib. This resinless section was located within the bending shear zone as shown in Figure 1a. The average maximum bending load value served as the control load to determine the fatigue levels of 50, 60, 70, and 80%. For this study, the maximum number of cycles was 10^6. There were also three wESCPs that were fatigue tested, one at each load level of 50, 60, and 70%. The laboratory environment during the test was around 65±3% RH and 23±3°C.

Static bending test: Three panels were (45 kN load cell on an Instron 5587 Test Machine) were performed according to the four point load configuration, ASTM C393-06, with cross-head speed of 5 mm-min^{-1}. The maximum bending deflection at mid-span was measured by a linear variable differential transformer (LVDT); Figure 1c shows a panel during loading.

The face and core shear bending stresses could be determined using equations from ASTM C393-06. However, the shear stress equation in the standard assumes an equivalent solid core configuration. This equation was inadequate for determining equivalent shear stress for the linear ribs of the core used in this study. Therefore, the equation was modified for an equivalent I-beam structure based on the equivalent shear stiffness.

$$\tau_{\text{rib}}=\beta\frac{P}{(d+c)b} \tag{1}$$

Where P is the applied load, d is the sandwich total thickness, c is the core thickness, and b is the panel width. β is the equivalent shear stiffness ratio, which can be written as:

$$\beta=\frac{A_S}{A_I} \tag{2}$$

Where A_S is the cross-sectional area of equivalent solid core based on standard, and A_I is the cross-sectional area of equivalent I-beam of tri-axial structural core (Li et al. 2013).

The bending stiffness can be determined by Eq. 3:

$$D=\frac{\text{slope}\cdot a}{48}(3l^2-4a^2) \tag{3}$$

Where the slope is the 20–40% ratio of the applied load P to mid-span deflection, l and a represent the bending span and the distance from the support to the load point, respectively.

Fatigue test: The 12 panels were fatigue tested based on ASTM D7774-12 at four load levels with three replicates for each level (MTS 204.12 machine with a servo-hydraulic load control actuator with a compression/tension capacity of ±17.8 kN). The set-up details were the same as for the statically tested panels. The cycle duration was 1 Hz due to the capacity of the hydraulic servo controller. Cyclic loading levels were determined on 50, 60, 70, or 80% of the maximum static bending load and were applied for each group in the fatigue tests, respectively. The servo signal was sinusoidal with a constant amplitude load ratio R=0.1. As the maximum load increased for each of the four levels, the minimum load also increased slightly as being 10% of that load. The fatigue test ended after 10^6 cycles. If a panel did not fail after 10^6 cycles, they were re-tested statically to bending failure. These data were called residual bending (RB) properties.

Fatigue damage test: Three panels with an initially "weakened" rib (wESCP) were tested by means of the same procedure as described above for 50, 60, and 70% maximum static load levels.

Results and discussions

Static bending properties

Figure 2 shows the plots of load and mid-span deflection of three ESCPs and their average for static bending. The average failure load was 11.6 kN with 31.4 mm maximum deflection at the mid-span (Table 1). The average face stress of 70.4 MPa, was determined as the ultimate materials' strength for compression failure on the face (Figure 3a). The core shear stress was calculated as an equivalent I-beam for the rib of core using Eq. 2 based on equivalent shear stiffness (Li et al. 2013).

The primary failure for panels in static bending occurred in the pure bending zone (Figure 3a) either in compression on the top face or in tension on the bottom face. Total failure stress of either face compression of 195 MPa or tension of 173 MPa was reached before the core shear stress limit of 17.9 MPa at the core/face interface (epoxy resin) was reached in the shear zone of the panel (Li et al. 2016a). The core rib material's shear stress limit was 84.1 MPa, almost four times the shear stress capacity of the resin. The static core/face interface interaction associated with the epoxy interface resisted shear failure forcing failure to occur in compression or tension.

Fatigue properties

The 12 panels were fatigue tested at the four stress levels or three panels at each stress level. The data are summarized in Table 2. The bending loads for the fatigue tests at the 50, 60, 70, and 80% load levels were 5.6 kN,

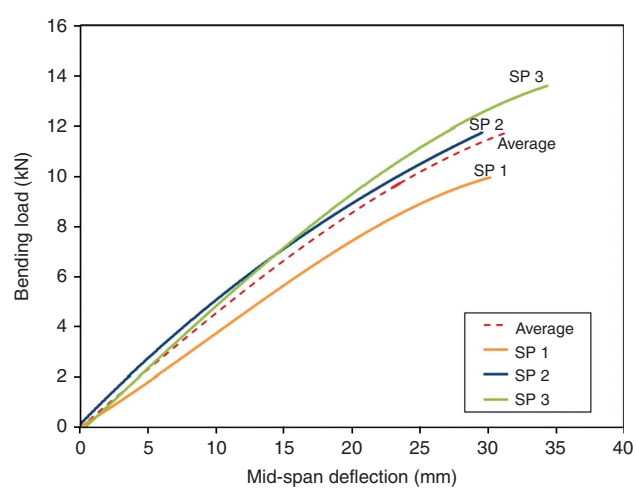

Figure 2: Static load vs. deflection for three panels.

Brought to you by | DigiTop - USDA's Digital Desktop Library
Authenticated
Download Date | 11/23/15 11:09 PM

Table 1: Static bending characteristics of ESCP.

Group A	Bend. load, F_{max} (kN)	Max defl. Δ_{max} (mm)	Face stress, σ_{face} (MPa)	Core stress, τ_{rib} (MPa)	Bending stiffness, D (kN·m²)
SP 1[a]	9.9	30.2	62.8	14.9	5.59
SP 2	11.6	29.6	68.8	17.5	6.68
SP 3	13.4	34.4	79.6	20.4	6.10
Avrg.	11.6	31.4	70.4	17.6	6.12
	(12.1)[b]	(6.7)	(9.9)	(12.7)	(7.4)

[a]SP Panel submitted to static test. [b]% Variation.

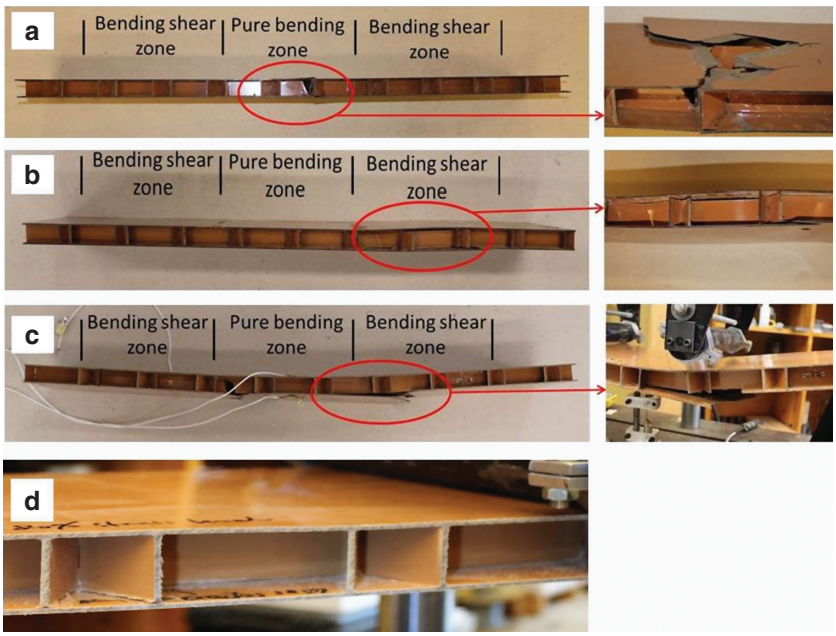

Figure 3: (a) Static bending failure mode, (b) fatigue failure mode, (c) residual tested failure mode of the panel after 1 million cycles at 50% stress level, (d) typical cracks at the core:face interface for the fatigue panel prior to failure.

Table 2: Average fatigue characteristics of test groups.

	Face properties		Fatigue load properties		
Test method	Face stress (MPa)	Equiv. core stress (MPa)	Max. load (kN)	Min. load (kN)	Cycles (N)
Static	70.4 (9.9)[a]	0.62 (12.3)[a]	–	–	–
50%	35.2	0.29	5.6	0.56	10^6
60%	42.2	0.35	6.7	0.67	225 857 (51.6)[a]
70%	49.3	0.41	7.8	0.78	76 557 (93.7)[a]
80%	56.3	0.46	8.9	0.89	35 231 (78.6)[a]
50% (wESCP)	35.2	0.35	5.6	0.56	81 813 (8)[b]
60% (wESCP)	42.2	0.41	6.7	0.67	33 946 (15)[b]
70% (wESCP)	49.3	0.46	7.8	0.78	4032 (5)[b]

[a]Coefficients of variation, in percent. [b]% Of fatigue cycles for wESCP vs. ESCP.

6.7 kN, 7.8 kN, and 8.9 kN, respectively. The minimum fatigue load for each group was calculated by the amplitude load ratio of R=0.1. The results from the fatigue life, Figure 4a, show that at a 50% maximum load level, the panels have a fatigue life above 10^6 cycles. The panels cyclically loaded to 60% stress level failed after 225 857 cycles. When the stress level was increased to 70%, the fatigue life dramatically decreased to 76 557 cycles. At

Brought to you by | DigiTop - USDA's Digital Desktop Library
Authenticated
Download Date | 11/23/15 11:09 PM

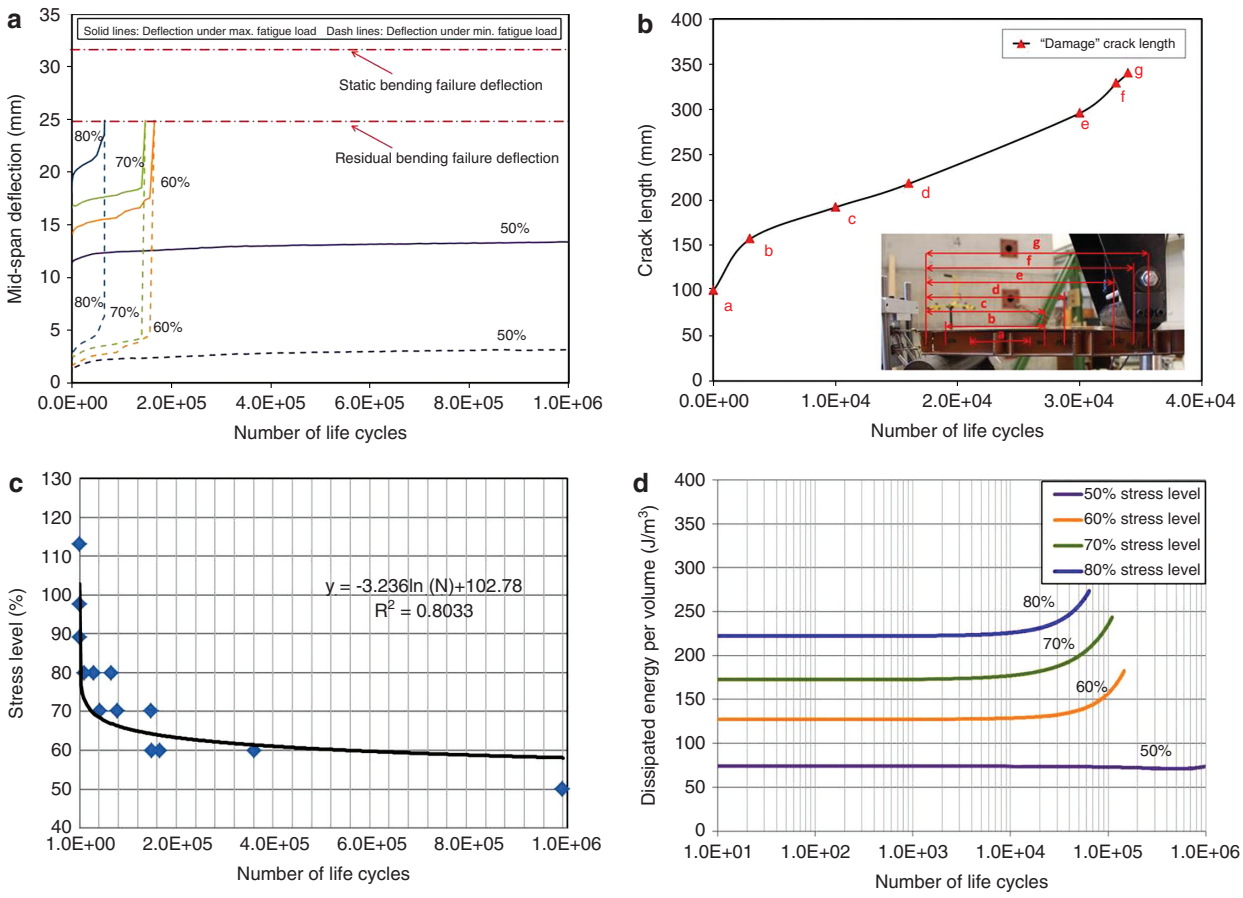

Figure 4: Fatigue behaviors as a function of cycles. (a) typical panel mid-span deflections at 50%, 60%, 70%, and 80% stress. Static bending and residual bending mid-span panel deflections are shown for comparison, (b) crack length for the wESCP at 60% stress level, (c) stress level degradation regression, (d) typical dissipated energy per volume under different stress levels.

80% stress level, the fatigue life was further reduced to 35 231 cycles. As expected, the deflections for the initial fatigue panels exhibited similar deflections as obtained at the same load level for the panels under static bending (Figure 2). Figure 4a also shows that the panels loaded at the 50% stress level only increased 4.9% relative displacement as it approached 10^6 cycles. However, for stress levels of 60, 70, and 80%, the deflection rate increased as load levels increased. Obviously, the higher stress levels had an increasing effect on deflection and accumulated damage. To reduce the data file size for each test, deflection data was only captured for a decreasing number of cycles with increasing cycle count. Deflection data were collected cycle-wise from the 1th to 100th cycles; every 10^2 cycles from 10^2 to 10^3 cycles; every 10^3 cycles from 10^3 to 10^4 cycles, etc. Since failure did not occur exactly on one of these data collection cycles, the final deflection line was drawn as a straight line to the static residual bending failure deflection point at the last known total cycle number, thus indicating failure.

All "fatigue panels" had a similar failure mode. Random small cracks slowly developed at the core/face interface in the bending shear zone until major cracks began to occur. As load increased, major cracks rapidly propagated along the core/face interface primarily along the longitudinal direction. The panels did not fail immediately even though the presence of cracks was readily visible. At some point, failure occurred suddenly within the epoxy. There was also evidence of surface debonding failure within the laminate between the core/face interfaces (Figure 3d).

Residual bending (RB) properties

At the 50% load level, the panels had not reached failure after 10^6 cycles. These panels were then tested in static bending to determine the residual bending (RB) properties compared to the properties obtained at the initial static bending test. The data concerning maximum failure

Brought to you by | DigiTop - USDA's Digital Desktop Library
Authenticated
Download Date | 11/23/15 11:09 PM

Table 3: Residual bending (RB) properties for the non-failed panels at 50% stress level after 10^6 cycles.

Residual bending	Bending load F_{max} (kN)	Max. defl. Δ_{max} (mm)	Face stress, σ_{face} (MPa)	Core stress, τ_{rib} (MPa)	Bending stiffness *EI* (kN·m²)
RB 1	9.8	22.5	62.0	14.9	6.18
RB 2	11.1	29.0	70.2	16.9	5.93
RB 3	12.4	23.1	78.4	18.6	6.12
Avrg.	11.1	24.9	70.2	16.8	6.07
	(9.5)[a]	(11.8)	(9.6)	(9.1)	(1.8)
Δ[b]	4.4	20.8	0.2	4.3	0.7

[a]Coefficient of variation, (%). [b]Difference to static bending, Table 1 (%).

load, deflection, face stress, core stress, and bending stiffness for these panels are listed in Table 3. It is important to notice that the average values indicated that the properties of these RB panels were only around 5% lower than the values of the initial static bending tests. However, the average maximum deflection of the RB panels was 20.8% lower than those that had been only statically tested. This counter intuitive result could be explained based on "absolute displacement". The RB panels, after 10^6 cycles, had a final curvature or deflection due to cyclic damage as visible in Figure 4a. Therefore, the maximum strain-to-failure included the initial curvature plus the static deflection at failure. Because these RB panels had been removed from the test apparatus and then re-tested, it would be difficult to reconstruct their potential initial zero-load deflection. The small diagonal cracks in the epoxy interface observed with the panels in the fatigue tests may have contributed to the lower total failure loads. It is also possible that the small cracks provided better stress "redistribution" so that all components shared the load, as compared to a more rigid original panel without micro-cracks.

The typical failure mode for the RB panels was interface shear in the shear zone (Figure 3c), whereas the static bending panels failed in the pure bending zone (Figure 3a), as described above. The panels in fatigue tests had developed small cracks in the epoxy at the core/face interface throughout the shear zone so that failure occurred when shear loads reached levels that could not be restrained by the cracked epoxy.

Fatigue properties of weakened panels (wESCP)

The panels with an artificially weakened rib (wESCP, obtained by omission of the resin along a 100 mm long section of the rib) served for comparison for the core/face interface failure zone with those of the ESCP. The wESCPs were prepared to force crack propagation for a better visibility of a failure mechanism at a known location. The cyclic percentage ratio, wESCP/ESCP at 50, 60, and 70% stress levels failed at cycle percentage ratios of 8, 15, and 5%, respectively (Table 2). Figure 4b shows damaged crack length propagation as a function of cycles for the 60% stress level fatigue tested panel. Initially, the crack length propagated quickly causing the damaged panel to fail with only 15% of the total number of cycles for the ESCP. These results show that the damaged section quickly propagated causing premature failure if a section of the core/face interface is not well bonded. For the ESCP, the cracks propagated randomly, whereas the crack propagation failure mechanism was observed on the wESCP at a prescribed location. While care was taken during the ESCP fabrication process, it is possible that some of the experimental data variation was due to the random defects from manual fabrication techniques when adhering the face to core.

The wESCPs and ESCPs have similar failure modes, but the crack propagation in the former is initiated by the absence of epoxy and propagated along the interface as cyclic loading occurred. The weakened portion within the epoxy minimized the small-crack stage. The crack propagation of wESCP at the cyclic loading of 60% maximum stress level is shown in Figure 4b. It was observed that the initial 100 mm crack nonlinearly propagated with increasing number of cycles and reached a length of 350 mm before failure (corresponding 38% of the total span). The other two wESCPs at 70 and 80% stress levels as the former one.

Fatigue damage analyses

Normalized damage as a function of relative life cycle for panels at 60, 70, and 80% stress levels are presented in Figure 5a. The normalized damage scale was calculated as a ratio of the loss in mid-span deflection:

Brought to you by | DigiTop - USDA's Digital Desktop Library
Authenticated
Download Date | 11/23/15 11:09 PM

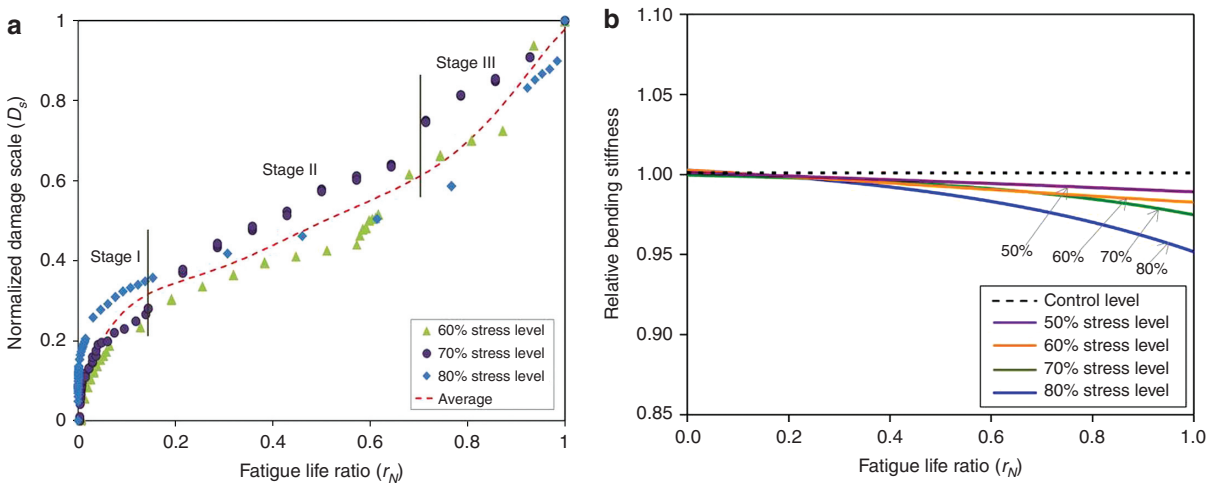

Figure 5: Fatigue behaviors as a function of fatigue life ratio. (a) Normalized damage for fatigue panels. (b) Typical relative bending stiffness for panels under different stress levels.

$$D_S = \frac{d_{r_N} - d_{r_0}}{d_t - d_{r_0}} \tag{4}$$

Where d_{r_N} is the maximum mid-span deflection at cycle N; d_{r_0} is the initial maximum mid-span deflection for cycle 1 and d_t is the maximum mid-span deflection at the failure cycle. The fatigue life ratio was calculated by:

$$r_N = \frac{N}{N_t} \tag{5}$$

Where N is the fatigue cycle, and N_t is the total fatigue cycle for each panel. Stage I was defined as the non-linear portion where sub-structures failure and stress redistribution occurred. Transition to stage II occurred between 0.1 and 0.2 of fatigue life ratio. Stage II is defined as the linear accumulation of damage as a function of cycles. This stage consists of approx. 60% of the total fatigue life. Stage III is defined as the non-linear accelerated damage as cycles increased. At this point, major cracks were developing and could be observed in the epoxy until the core/face interface could not support any further shear stresses and failure occurred. Stage III occurred approx. after the damage had reached 0.6–0.7 total fatigue life. The 50% stress level panel did not reach stage III even after 10^6 cycles. At least for this panel construction, without an initial damaged section, 10^6 cycles were not sufficiently long to begin stage III behavior.

Fatigue bending stiffness degradation

The relationships for relative bending stiffness degradation for the panels under different stress levels are presented in Figure 5b. As visible, only slight stiffness degradation occurred during the fatigue life time. The maximum degradation was around 5% less for the panels at 80% stress level compared with the static load. This decrease was after about 4×10^4 cycles. For the panel at 50% stress level, there was approximately 1% decrease at the end of 10^6 cycles. A rapid increase in deformation increased for the last several cycles before failure. At the higher loads, debonding (cracks) in the core/face interfaces were decoupled so that stiffness quickly decreased due to the bending load transfer degraded till failure.

Fatigue regression model

One objective was to determine an approximate relationship between applied stress and fatigue life, S-N. The experimental data implies that a possible exponential relationship exists between these parameters. The following exponential equation might describe the relation:

$$S = A\ In(N) + B \tag{6}$$

Where S is the percentage of applied stress to the predicted static stress and N is the number of cycles-to-failure. A and B are constants that relate to the material properties.

The regression analyses helped determine constants A and B and their correlation coefficient R^2 (Figure 4c) is 0.8033. Presumably, correlation could have been better in case of not handmade panels, which contain inevitably small irregularities.

Fatigue energy dissipation

The typically dissipated energy was calculated by difference between the initial form of loading phase and final

Brought to you by | DigiTop - USDA's Digital Desktop Library
Authenticated
Download Date | 11/23/15 11:09 PM

form of releasing phase of each cycle. Figure 4d shows the fitted curves with this regard under different load amplitudes. These stiffened panels display an elastic behavior under bending fatigue loading while the hysteresis loop was very small in the fatigue tests. Accordingly, dissipated energy per volume in each stress level is also very small, particularly, under low load of 50% stress level without failure. Expectedly, the initial dissipated energy increased as fatigue bending load increased. For the panel under 50% stress level without failure, the dissipated energy showed a near linear characteristic during the entire fatigue life. However, the panel at increasing higher stress levels showed increasing dissipated energy per volume. The dissipated energy per volume vs. life cycles for both panels at 60 and 70% stress levels showed similar trends for panels under 80% stress level, but the curve's yield point was delayed to higher number of cycles. Probably, the number of cracks and severity of the cracks increased as a function of the total dissipated energy of each panel.

Conclusions

ESCP were fabricated and tested to investigate both static and fatigue bending properties by means of third point loading bending. The panels tested in the static bending tests failed in the faces in the pure bending zone while the panels tested in the fatigue tests failed in the core:face interface in the shear zone. The fatigue results showed that the panels at 50% stress level did not fail even after 10^6 cycles. As stress levels increased to 60% and above, the panels failed with decreasing fatigue cycles. The primary failure mode in the fatigue tests at 60, 70, and 80% stress levels was micro cracks in the epoxy resin or debonding observed in the shear zone, which was different from the static bending test, where face failure occurred in the pure bending zone. For the static RB tests, epoxy debonding failure occurred between the pure bending zone and shear zone. The normalized damage data shows crack propagation or damage, which can be described as a three stage damage process. The standard *S-N* diagrams were fitted to evaluate the fatigue performance. The dissipated energy of the panels was small due to the high stiffness of the materials, while the panels under higher stress level had larger dissipated energy growth ratio as life cycle increased compared to the panel under lower stress levels. To improve fatigue performance of these panels, an interface reinforcement method should be studied.

Acknowledgments: This work is supported by USDA, Forest Products Laboratory and the authors gratefully acknowledge the support of Sara Fishwild, James Bridwell, Marshall Begel, Dave Simpson, and Marc Joyal of EMRSL group for the mechanical testing.

References

ASTM standard (2006) C393, Test method for core shear properties of sandwich constructions by beam flexure.

ASTM standard (2012) D7774, Standard test method for flexural fatigue properties of plastics.

Bao, Z., Eckelman, C., Gibson, H. (1996) Fatigue strength and allowable design stresses for some wood composites used in furniture. Holz. Roh. Werkst. 54:377–382.

Belingardi, P., Martella, P., Peroni, L. (2007) Fatigue analysis of honeycomb-composite sandwich beams. Compos. A 38:1183–1191.

Bianchi, G., Aglietti, G.S., Richardson, G. (2012) Static and fatigue behavior of hexagonal honeycomb cores under in-plane shear loads. Appl. Compos. Mater. 19:97–115.

Cai, Z.Y., Bradtmueller, J.P., Hunt, M.O., Fridley, K.J., Rosowsky, D.V. (1996) Fatigue behavior of OSB in shear. Forest Prod. J. 46:81–86.

Cicala, G., Recca, G., Oliveri, L., Perikleous, Y., Scarpa, F., Lira, C., Lorato, A., Grube, D.J., Ziegmann, G. (2012) Hexachiral truss-core with twisted hemp yarns: out-of-plane shear properties. Compos. Struct. 94:3556–3562.

Davalos, J.F., Qiao, P.Z., Xu, X.F., Robinson, J., Barth, K.E. (2001) Modeling and characterization of fiber-reinforced plastic honeycomb sandwich panels for highway bridge applications. Compos. Struct. 52:441–452.

Eckelman, C.A., Winandy, J.E. FEHS-78-125, The Performance Test Method for Upholstered Furniture. Federal Supply Service, General Services Administration. Washington, DC, 1978.

Fan, H.L., Meng, F.H., Yang, W. (2007) Sandwich panels with kagome lattice cores reinforced by carbon fibers. Compos. Struct. 81:533–539.

Gan, C., Gibson, R.F., Newaz, G.M. (2004) Analytical/Experimental investigation of energy absorption in grid-stiffened composite structures under transverse loading. Exp. Mech. 44:185–194.

Gibson, L.J., Ashby, M.F. Cellular Solids: Structure and Properties. Cambridge University Press, Cambridge, 1997.

Han, D.Y., Tsai, S.W. (2003) Interlocked composite grids design and manufacturing. J. Compos. Mater. 37:287–316.

Higgins, J., Wegner, P., Viisoreanu, A., Sanford, G. (2004) Design and testing of the Minotaur advanced grid-stiffened fairing. Compos. Struct. 66:339–349.

Huybrecht, S.M., Meink, T.E., Wegner, P.M., Ganley, J.M. (2002) Manufacturing theory for advanced grid stiffened structures. Compos. A 33:155–161.

Jen, Y.M., Ko, C.W., Lin, H.B. (2009a) Effect of thickness of face sheet on the bending fatigue strength of adhesively bonded aluminum honeycomb sandwich beams. Eng. Fail. Anal. 16:1282–1293.

Jen, Y.M., Ko, C.W., Lin, H.B. (2009b) Effect of the amount of adhesive on the bending fatigue strength of adhesively

Brought to you by | DigiTop - USDA's Digital Desktop Library
Authenticated
Download Date | 11/23/15 11:09 PM

bonded aluminum honeycomb sandwich beams. Int. J. Fatigue 31:455–562.
Li, J.H., Hunt, J.F., Cai, Z.Y., Zhou, X.Y. (2013) Bending analyses for 3D engineered structural panels made from laminated paper and carbon fabric. Compos. B 53:17–24.
Li, J.H., Hunt, J.F., Gong, S.Q., Cai, Z.Y. (2014) High strength wood-based sandwich panels reinforced with fiberglass and foam. Bioresources 9:1898–1913.
Li, J.H., Hunt, J.F., Gong, S.Q., Cai, Z.Y. (2016a) Simplified analytical model and balanced design approach for light-weight wood-based structural panel in bending. Compos. Struct. 136:16–24.
Li, J.H., Hunt, J.F., Gong, S.Q., Cai, Z.Y. (2016b) Testing and evaluation of a slot and tab construction technique for light-weight wood-based structural panels under bending. Submitted to ASTM J. Test. Eval. 44:1–10.
Nakano, T. (1997) Fatigue and heating in the non-linear region for wood. Holzforschung 51:309–315.
Shalbafan, A., Lüdtke, J., Welling, J., Frühwald, A. (2013) Physiomechanical properties of ultra-lightweight foam core particleboard: different core densities. Holzforschung 67:169–175.
Sharaf, T., Fam, A. (2011) Experimental investigation of large scale cladding sandwich panels under out-of-plane transverse loading for building applications. J. Compos. Constr. 13:422–430.
Smardzewski, J. (2013) Elastic properties of cellular wood panels with hexagonal and auxetic cores. Holzforschung 67: 87–92.
Vasiliev, V.V., Barynin, V.A., Rasin, A.F. (2001) Anisogrid lattice structures survey of development and application. Compos. Struct. 54:361–370.
Wei, X., Tran, P., De Vaucorbeil, A., Ramaswamy, R.B., Latourte, F., Espinosa, H.D. (2013) Three-dimensional numerical modeling of composite panels subjected to underwater blast. J. Mech. Phys. Solids 61:1319–1336.
Wodesenbet, E., Kidane, S., Pang, S.S. (2003) Optimization for buckling loads of grid stiffened composite panels. Compos. Struct. 60:159–169.
Zhang, J.F., Zhang, B.M., Du, S.Y. (2005) Design and manufacture of improved interlocked composite grid structures. In: Composite Materials, Proceedings of the 3th International Conference on Composites in Construction. Lyon, France. pp. 693–701.
Zuhri, M.Y.M., Guan, Z.W., Cantwell, W.J. (2014) The mechanical properties of natural fibre based honeycomb core materials. Compos. B 58:1–9.

Brought to you by | DigiTop - USDA's Digital Desktop Library
Authenticated
Download Date | 11/23/15 11:09 PM